Upcycling spent coffee grounds and waste PET bottles into electrospun composite nanofiber mats for oil structuring applications

J.F. Rubio-Valle, C. Valencia, M.C. Sánchez, J.E. Martín-Alfonso, J.M. Franco ✉

Pro2TecS – Chemical Product and Process Technology Research Center, Department of Chemical Engineering and Materials Science, Universidad de Huelva, ETSI, Campus de "El Carmen", 21071 Huelva, Spain.

✉ Corresponding author:
Prof. J.M. Franco, Dept. Chemical Engineering and Materials Science, ETSI, Campus de "El Carmen". Universidad de Huelva, 21071 Huelva, Spain.
Phone: +34 959 219995; e-mail: franco@uhu.es

Abstract

Spent coffee grounds (SCG) and post-consumer PET bottles (PETbot) are major waste materials from the food industry. In this work, their use to obtain electrospun composite nanofibers is explored aiming to develop a new route for their upcycling into high added-value oil-based products. Raising the proportion of PETbot increased the average fiber diameter (from 0.36 to 0.89 μm) and enhanced the tensile properties of the mats. Young's modulus and strain-at-break increased from 5.1 to 32.8 MPa and from 13.8 to 39.4%, respectively, as the SGC:PETbot weight ratio decreased. Dispersions of the mats in castor oil exhibited shear-thinning and gel-like viscoelastic properties which can be tuned through the SCG:PETbot ratio. Friction coefficient values of resulting oleogels tested in a tribological contact ranged from 0.165 to 0.092. SCG and PETbot can be used to obtain electrospun nanofibers with oil structuring capabilities while resulting oleogels are proposed as environmentally-friendly alternatives to semisolid lubricants.

Keywords: Electrospinning, Lignocellulose, Nanofibers, Oleogels, PET, Rheology, Waste.

1. Introduction

There is increasingly widely awareness that the traditional linear economy model, by which resources are collected and transformed into products and consumer goods for use until they are disposed of as waste, is making our planet unsustainable (Michelini et al., 2017). In stark contrast to nature's life cycle, the still prevailing linear economic system focuses on the short-term consumption, thus precluding sustainable development (Sarja et al., 2021). The concept of circular economy, inspired by nature's cyclical model, emerged strongly in the past decade to solve the ensuing problems. In circular economy, resources are managed and used more sustainably by having products and services in circulation for as long possible. The primary aim is to minimize production and, when a given product must unavoidably be used, to recycle and reuse it. Circular economy also advocates using as many biodegradable and/or renewable materials as possible (Camacho-Otero et al., 2018; Geisendorf and Pietrulla, 2018) to produce consumer goods. In those cases where using environmentally friendly materials or components is impossible, the aim is to give existing products a second life by recycling or, preferably, upcycling, i.e. by reinserting them into the production cycle in order to develop new added-value products (Morseletto, 2020; Webster, 2021).

The food, chemical and textile industries generate vast amounts of waste from the start of the production cycle through packaging to disposal by consumers (Reynolds et al., 2016; Sridhar et al., 2021; Thyberg and Tonjes, 2016). One salient example of waste from the food industry is spent coffee grounds (SCG) (Campos-Vega et al., 2015). This lignocellulosic waste has become an environmental concern because, unless disposed of appropriately, it can release caffeine, tannins and polyphenols resulting from coffee fermentation (Bomfim et al., 2022; Franca and Oliveira, 2022). SCG are generated as waste after infusion and account for about 90% of the initial mass of the beans. In 2022, global coffee production exceeded 10 million tons (Bomfim et al., 2022; Forcina et al., 2023). A number of efforts have been made over the last decade to valorize and/or repurpose this waste in eco-friendly ways in fields such as agriculture and biofuel energy production, and also in the production of polymer and composite

precursors (Kang et al., 2023; Nanni et al., 2022; Gupta et al., 2022), graphene (Dericiler et al., 2022) and other chemicals (Leow et al., 2021), dye sorbents (Kasbaji et al., 2023) or 3D printing materials (Yu et al., 2023), among other uses (Jin Ong et al., 2023; Pagett et al., 2023).

Plastic is one of the most common food packaging wastes from the food industry (Evode et al., 2021; Ncube et al., 2021). In fact, its role in food safety and preservation has turned it into an indispensable convenience. Global plastic production in 2021 amounted to 390.7 million metric tons, 4% over the figure for the previous year (Statista, 2023). Also, it is expected to continue to rise sharply and reach around 1.1 billion tons by 2050 (Naderi Kalali et al., 2023). The US Environmental Protection Agency (EPA) reports that only 7% of all plastic is recycled, of which 30% corresponds to used poly(ethylene terephthalate) (PET) bottles (Naderi Kalali et al., 2023).

Efficient recycling of plastic polymer waste has become a major priority worldwide (Shanmugam et al., 2020). In fact, post-consumer PET bottles (PETbot) are highly valued for producing a variety of polymeric and composite materials because they are much less expensive than virgin PET (Rosenboom et al., 2022; Smith et al., 2022). Recycled PET has thus emerged as a highly suitable, cost-effective choice for a wide variety of uses such as protective clothing, membranes, vascular grafts, tissue scaffolding and filtration media (Rahmati Nejad et al., 2020; Sadeghi et al., 2021; Tian and Mo, 2019).

Oleogelation and oil structuring have aroused much interest for a broad range of uses (Davidovich-Pinhas, 2016; Pakseresht and Mazaheri Tehrani, 2022; Patel, 2018, 2017) but particularly in the production of lubricants, coatings and adhesives (Gallego et al., 2015a; Raghunanan et al., 2018; Borrero-López et al., 2018;Tenorio-Alfonso et al., 2021, 2020). Increasing environmental awareness has raised a growing industrial concern with replacing petroleum based components with renewable and/or recycled materials. For instance, the lubricant industry is not only replacing conventional mineral oils with vegetable oils or glycerol esters (Panchal et al., 2017; Syahir et al., 2017), but also pursuing the development of semisolid lubricants and greases obtained by using

environmentally friendly oil structuring and thickening agents with specific rheological and tribological functionalities. This functional performance has traditionally been achieved by using metal soaps —lithium soaps, mainly (~80%)— and polyureas or other polymers from the petrochemical industry. However, given that global grease production is estimated at around 1.1 Mton/year (Lubes'n'Greases, 2021), and that the thickener content in greases typically ranges from 3% to 40% by weight, the search for technically efficient renewable or bio-sourced thickening agents is a challenging goal. One must also consider the significance of lithium to other more demanding and pressing uses such as batteries and the supply constraints on this scarce resource. Similar considerations also apply to oil-based adhesive and coating formulations (Bashir et al., 2022; Cheng et al., 2018; Sahoo et al., 2018; Tenorio-Alfonso et al., 2020). New oil structuring agents based on renewable and/or recycled materials are therefore needed to meet existing technical and environmental challenges.

In previous work, different approaches involving the chemical alteration of biopolymers to induce oil structuring via chemical crosslinking with isocyanate or epoxide reactive groups were followed (Borrero-López et al., 2017; Cortés-Triviño et al., 2021, 2018; Gallego et al., 2015a, 2013). Nevertheless, these modifications usually require using solvents and chemical reagents that make the synthesis of oil thickeners somewhat cumbersome and not entirely environmentally friendly. Very recently, nanostructures obtained by electrospinning unmodified lignocellulosic polymers to be effective oil structuring agents were assessed (Borrego et al., 2022, 2021; Rubio-Valle et al., 2023); however, some cospinning polymer was occasionally required to improve the morphology of the resulting electrospun nanofiber mats. The aim of this work is to investigate the use of a lignocellulosic waste material such as spent coffee grounds (SCG) to obtain electrospun nanofiber mats with potential oil structuring capabilities. Also post-consumer PET bottles were evaluated as a cospinning polymer to develop a new valorization or upcycling route for these waste materials that is fully aligned with the circular economy paradigm. It is the hypothesis of this work that the high aspect ratio and porosity of SCG/PETbot nanofiber webs can promote the formation of 3D

percolation networks that enhance the physical interactions with the oil and help stabilize the colloidal system. Moreover, the rheological properties of the oleogels derived should be tunable by varying the SCG:PETbot proportion. Finally, a potential application of these oleogels as semi-solid lubricants is explored in this work. Although PET from bottles has already been used as a component of electrospun membranes for various uses (Hossain et al., 2022; Strain et al., 2015), SCG has to the best of our knowledge never been used before to obtain electrospun nanofiber mats. In any case, neither material has been explored as an oil structuring agent for producing gel-like or soft materials. For a better and quick understanding of the whole process aimed at upcycling SCG and PETbot waste materials into oil structuring agents, finally leading to oleogels with potential lubricant applications, Scheme 1 displays a flow chart in which the sequence of the different stages followed can be readily visualised.

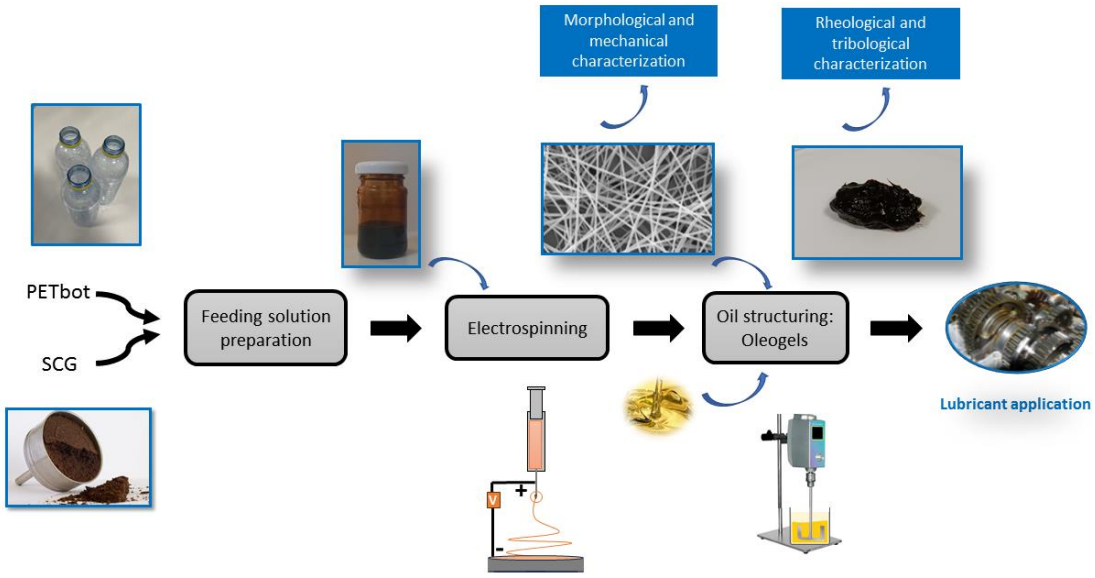

Scheme 1. Synopsis of the process to upcycle SCG and PETbot into oil structuring agents for lubricant applications and characterization methodologies followed.

2. Material and methods

2.1. Materials

SCG was collected from a local cafe in Huelva (Spain). The material was obtained by brewing Spanish Delta coffee and oven-drying it at 100 °C for 24 h. Previously collected post-consumer beverage bottles (PETbot, Fuenteliviana, Spain) were cleaned with household detergent and ultrapure water, dried in an oven at 100 °C for 24 h and cut into small (1−2 mm) pieces. Trifluoroacetic acid (TFA) for synthesis and dichloromethane (DCM, purity ≥ 99.5%), both supplied by Merck Sigma−Aldrich (Darmstadt, Germany), were used as solvents. Castor oil was purchased from Guinama (Valencia, Spain) and used as received. Compositional details and physical properties can be found elsewhere (Quinchia et al., 2010). Other general reagents used for chemical analysis were of analytical grade and also acquired from Merck–Sigma-Aldrich (Darmstadt, Germany).

2.2. Production of electrospun SCG/PETbot nanofiber mats

PETbot bottle pieces and SCG were dissolved in a 80:20 (v/v) TFA/DCM binary solvent at room temperature (22 ± 1 °C) under magnetic stirring at 650 rpm for 24 h. The total dissolved concentration was 15% (w/v) and the SCG/PETbot weight proportion 1:0, 2:1, 1:1, 1:2 or 0:1. The sample code used for each proportion is shown in Table S1 (see Supporting Information).

SCG/PTEbot solutions were used as feed streams in the electrospinning chamber (DOXA Microfluidics, Málaga, Spain), which were continuously pumped at a controlled flow rate of 0.8 mL/h through a plastic syringe furnished with a 20-G needle. The syringe was horizontally arranged and connected to a high-voltage power source that supplied 15 kV. Electrospun nanofibers were collected on an aluminum surface positioned 10 cm from the needle tip. Electrospinning was conducted at 22 ± 1 °C and 45 ± 1% relative humidity.

2.3. Preparation of oleogels

Electrospun SCG/PETbot nanofiber mats were carefully removed from the collector and directly dispersed at a 5 wt.% concentration in castor oil under gentle agitation (60 rpm) at room temperature for 24 h before storage, also at room temperature. The oil was first placed in an open vessel and nanofiber mats were slowly added and dispersed using an Ika-RW 20 (Staufen, Germany) mixing device fitted with an anchor impeller.

2.4. Characterization techniques

The chemical composition of SCG was established after a hydrolysis treatment with sulfuric acid at 30 °C. 5 mL of 72 wt.% sulfuric acid was added to an SCG aliquot (0.5 g) by gently stirring for 1 h. Subsequently, a post-hydrolysis with 4 wt.% sulfuric acid (by adding water) was carried out in autoclave at 121 °C for 60 min. The resulting solid residue was recovered by filtration and, based on Tappi T222, taken to be Klason lignin. Monosaccharides in the hydrolyzates were determined by HPLC at 30 °C, with an Aminex HPX-87H ion-exchange column as stationary phase and 0.005 M H_2SO_4 at a flow rate of 0.6 mL min^{-1} as mobile phase, according to Tappi T249 in order to estimate the glucan, xylan and arabinan contents. An Eltra CHS-580A Helios device (Verder Scientific, USA) was used for elemental analysis of SCG.

Fourier-transform infrared (FTIR) spectra for SCG, PETbot and nanofiber mats were acquired with an FT/IR 4200 instrument from Jasco, Inc. (Tokyo, Japan) over the wavenumber range 4000−400 cm^{-1} (4 cm^{-1} resolution and 200 scans per spectrum). For this, the samples were placed in an attenuated total reflectance (ATR) accessory furnished with a monolithic diamond crystal.

Thermogravimetric analyses (TGA) were carried out on a Q50 thermogravimetric analyzer from TA Instruments (New Castle, DE, USA). An amount of 4−7 mg of sample was placed on a platinum pan and heated from 30 to 600 °C at 10 °C·min^{-1} under an N_2 stream (flow rate, 100 mL/h).

The morphology of electrospun nanofiber mats was examined in a JXA-8200 SuperProbe scanning electron microscope (SEM) from JEOL (Tokyo, Japan), using an acceleration voltage of 15 kV. The morphological observations were displayed at

× 4000 and × 10 000 magnifications. Previously, samples were gold sputtered in a BT150 sputter coater from HHV (Crawley, West Sussex, UK). Oleogels were analyzed microstructurally by using an AURIGA SEM apparatus from Zeiss (White Plains, NY, USA), using an acceleration voltage of 20 kV. The oleogels were previously subjected to chemical fixation (Pathan et al., 2010) and then sputtered with a thin layer of gold to improve the quality of the observations (Stokroos et al., 1998). SEM images were analyzed with the FIJI ImageJ software to determine some morphological parameters such as the average fiber diameter. Each sample was analyzed from 100 random observations at an identical magnification.

Electrospun nanofiber mats were subjected to uniaxial tensile tests on an AG-IS Universal Testing Machine from Shimadzu Corp. (Kyoto, Japan), equipped with a 50 N load cell, at room temperature (22±1 °C). The extensional rate applied was 0.1 mm s^{-1}. Samples were cut into rectangles 12.5 × 30 mm (~0.5 mm width) in size and placed in the metal clamps with sandpaper to prevent slippage. The measurements thus made allowed the maximum stress, strain at break and Young's modulus to be determined.

The rheological properties of the oleogels were examined with a Rheoscope controlled-stress rheometer from Thermo Fisher Scientific (Waltham, MA, USA), using a serrated plate-plate geometry (20 mm diameter, 1 mm gap). Viscous flow measurements were conducted by applying an increasing stepped shear rate ramp (3 min per point) from 10^{-2}–10^{2} s^{-1}. Small-amplitude oscillatory shear (SAOS) tests were carried out within the linear viscoelastic region in the 0.03−100 rad s^{-1} frequency range. Prior to this, the extension of the linear viscoelastic range was determined by performing stress sweep tests. All rheological measurements were made at 25 °C.

Tribological tests were conducted on a Physica MCR-501 rheometer from Anton Paar (Graz, Austria) furnished with a tribological cell containing a steel ball 6.35 mm in diameter that was rotated on three 45° inclined rectangular steel plates where the oleogel samples were placed and tested as lubricants. A constant normal load of 20 N on the inclined plates and a rotational speed of 10 rpm were applied for 10 min. Tribological tests were performed under mixed lubrication and pure sliding conditions.

The tribological cell adapted to the rheometer allows the coefficient of friction to be calculated as the ratio between the measured friction force and the applied normal load. The effective normal force and sliding velocity were calculated from the applied axial force, ball radius, and angular velocity as shown elsewhere (Heyer and Läuger, 2009). The wear marks produced on the steel plates were examined with a BX51 Olympus optical microscope (Tokyo, Japan) and the mean diameters were measured from the images.

2.5. Statistical analysis

The data underwent ANOVA analysis, with a minimum of three replicates for each independent measurement. Furthermore, a post hoc means comparison test was conducted to reveal any statistically significant differences ($p < 0.05$).

3. Results and discussions

3.1. Mat morphology

Figure 1 shows the morphologies of selected nanostructures obtained by electrospinning SCG/PETbot solutions in variable SGC:PETbot weight ratios. As can be seen, electrospinning an PETbot-free SCG solution produced no nanofibers but only microsized electrosprayed particles (see Figs 1a and 1b). These results are consistent with others previously obtained by electrospinning lignin fractions (Borrego et al., 2021; Dallmeyer et al., 2010), which found that adding a cospinning or dopant polymer was essential for uniform bead-free nanofibers to form.

Linear polymers such as PET are easier to electrospin than heterogeneous, branched or low-molecular-weight polymers such as dissolved lignocellulosic fractions, which cannot entangle properly (Rubio-Valle et al., 2021; Svinterikos et al., 2020). Consequently, increasing the PETbot fraction in the electrospinning solutions helped obtain and stabilize jet formation, thus significantly reducing the number of isolated or embedded submicron particles. As shown by Figs 1c and 1d, adding PETbot to SCG in a 1:2 SCG:PETbot ratio led to a highly homogeneous nanofiber network containing

some beaded nanofibers or embedded micrometric particles. Further increasing the PETbot content (to a 1:1 SCG:PETbot ratio) almost completely avoided the formation of beaded fibers and led to rather homogeneous nanofiber mats with an increased fiber density (see Figs 1e and 1f) which, however, exhibited some surface texture or roughness as a result of the Taylor cone still being unstable to some extent owing to the contribution of SCG. This result is also consistent with those of other studies on the electrospinnability of lignocellulosic materials (Baker and Rials, 2013; Dallmeyer et al., 2014). Finally, the solution containing SGC and PETbot in a 1:2 weight ratio produced highly uniform nanofiber mats (Figs 1g and 1h) that were very similar to those obtained with PETbot alone (i.e., from the SCG-free solution) (Figs 1i and 1j), although they still contained some nanofiber beads (see, for instance, Fig. 1h). Figure 1 also shows the average nanofiber diameter as calculated from the SEM images. As can be seen, the higher the PETbot proportion was, the higher was fiber diameter as a result of fewer beads forming.

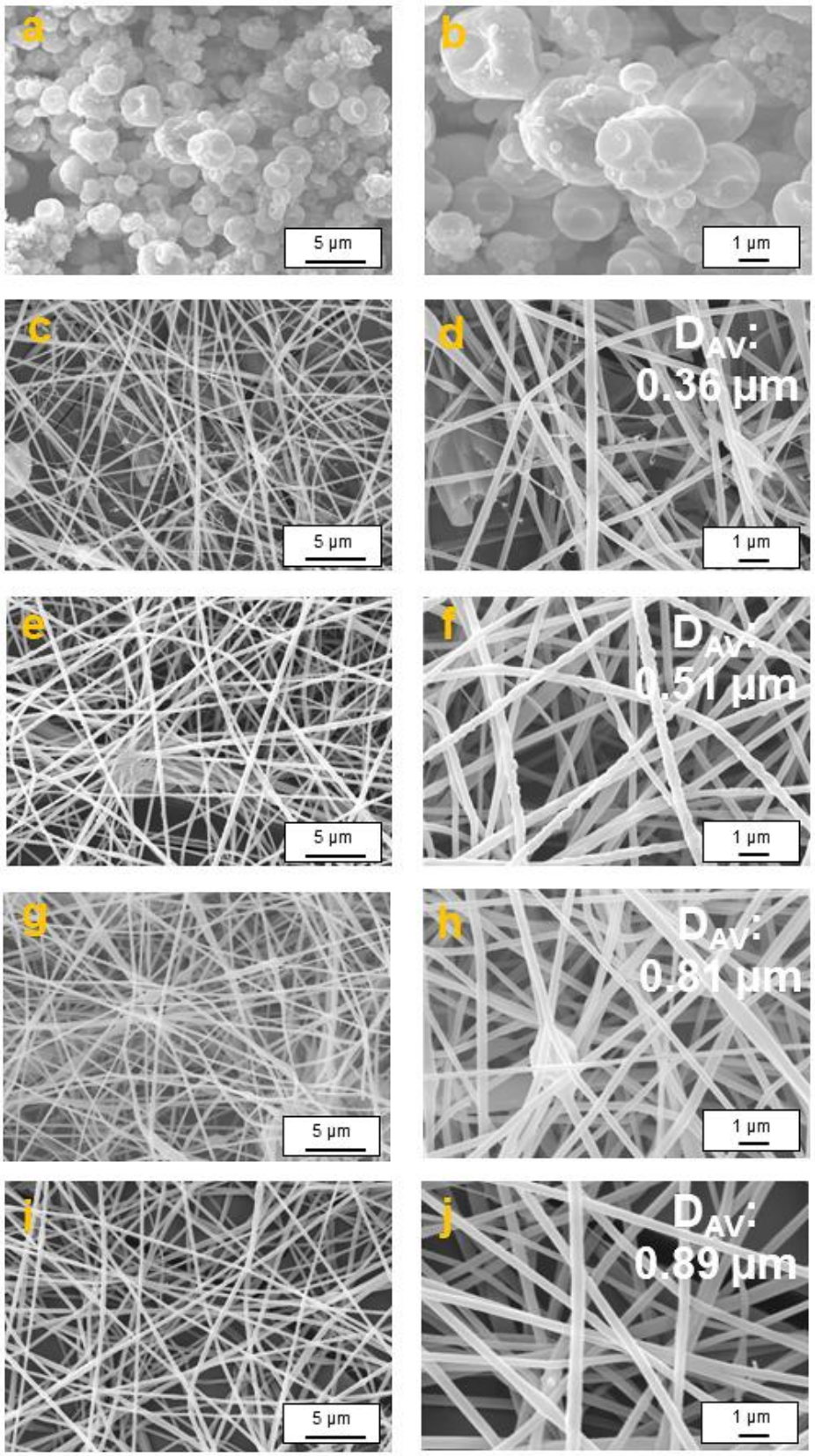

Figure 1. SEM images of SGCs/PETbot electrospun nanostructures obtained from solutions containing a 15 wt.% total polymer concentration in different SGC:PETbot weight ratios. (a), (b) 1:0. (c), (d) 2:1. (e), (f) 1:1. (g), (h) 1:2. (i), (j) 0:1. Magnification: × 4000 (left), × 10 000 (right).

3.2. Chemical and thermogravimetric analyses of the mats

The composition of the composite nanofiber mats was checked by FTIR spectroscopy and TGA analysis. Figure S1 (Supporting Information) shows the FTIR spectra for electrospun nanofiber mats obtained at different SGC:PETbot weight ratios as compared with the starting materials (SCG and PETbot). The main peaks associated with the chemical structure of PETbot were those corresponding to the ester C=O bond at 1714 cm^{-1}; the C=C stretching vibrations of the aromatic skeleton at 1577 and 1506 cm^{-1}; those of the terephthalate group ($OOCC_6H_4$–COO) at 1238 cm^{-1}, the methylene group at 1090 cm^{-1} and the ester C–O bond at 1016 cm^{-1}; and the wagging vibrations of C–H bonds in the aromatic structure at 722 cm^{-1} (Pereira et al., 2017). Consistent with its chemical composition (see Table S2, Supporting information), the FTIR spectrum for SGC exhibited a broad band at 3355 cm^{-1} typically attributed to stretching vibrations in O–H groups forming inter- and intramolecular hydrogen bonds in polymers such as cellulose, hemicellulose and lignin; two bands at 2923 and 2849 cm^{-1} due to asymmetric and symmetric C–H stretching vibrations; another two at 1515 and 1459 cm^{-1} due to aromatic skeleton vibrations in lignin; and a further two at 1070 and 1006 cm^{-1} that can be assigned to C–O bonds in lignin and cellulose, respectively (Davila-Guzman et al., 2016). The presence of hemicellulose polysaccharides was confirmed by a peak at 1737 cm^{-1} due to stretching vibrations in C=O groups (Nieva et al., 2019).

Both waste materials contributed to the FTIR spectra for the electrospun SCG/PETbot nanofibers, which exhibited the above-described bands and were consistent with those for sisal lignocellulose/PETbot fibers (Santos et al., 2015). For instance, the broad band at ca. 3600 cm^{-1} corresponding to hydroxyl groups in SCG, and those for C–H asymmetric and symmetric stretching vibrations at ca. 2918 and 2852 cm^{-1}, respectively, were quite apparent. Also, the peaks at ca. 1515 cm^{-1} and 1460 cm^{-1} can be assigned to aromatic skeletal vibrations in lignin and PETbot, while the band at ca. 1721 cm^{-1}, corresponding to the C=O bond of hemicellulose acetyl groups, was overlapped with that due to the ester group in PETbot. Bands due to the

terephthalate group and C–H vibrations in the aromatic structure of PETbot were also apparent. More important, no signs of degradation of the starting waste materials were detected.

Figure S2 (see Supporting Information) shows the TGA curves for electrospun SCG/PETbot nanofibers and also those for the starting PETbot and SCG materials. The temperature at the beginning of the degradation step (T_{onset}), that at which the decomposition rate peaked (T_{max}) and the weight loss in each degradation step, as well as the final proportion of residue remaining, were estimated from the thermograms for the samples (see Table 1). Thermal degradation of PETbot from post-consumer plastic bottles occurs in a single stage at T_{max} = 401 °C and results in a weight loss of 80% corresponding to decomposition of the polymer (Das and Tiwari, 2019). On the other hand, SCG degrades in three stages at a T_{max} of around 300, 333 and 395 °C, with a mass loss of 31, 18 and 19%, respectively, through depolymerization and decomposition of the main components of SCG (hemicellulose, cellulose and lignin; Brachi et al., 2021). The profiles for the thermal degradation of electrospun SCG/PETbot nanofibers, which also occurs in three stages if the initial weight loss due to residual solvent is neglected, confirmed that the proportions of SCG and PETbot were as intended. Thus, given that the main PETbot thermal degradation event roughly overlapped with the third degradation stage of SCG over the T_{max} range 395−427 °C, an increase in weight loss, together with a slight shift of the peak to 427 °C, was observed as the PETbot proportion was raised. On the other hand, the weight loss in the second thermal event (ca. 300 °C) increased with increasing SCG content. Finally, the proportions of residue in the electrospun nanofibers were similar to those of PETbot but lower than those of SCG, which indicates that part of the residue, especially in SCG, was not dissolved in the electrospinning solution.

Table 1. TGA characteristic parameters for electrospun SCG/PETbot mats and the starting waste materials (PETbot and SCG).

Samples	T_{onset} (°C)	T_{max} (°C)	Weight loss (%)	Residue (%)
PETbot	401	427	80	17
SCG	266/323/392	300/333/395	31/18/19	27
2SCG:1PETbot	158/271/415	240/300/399	8/30/40	17
1SCG:1PETbot	199/279/388	242/298/415	10/18/55	13
1SCG:2PETbot	208/282/398	248/300/425	7/10/65	14

3.3. Mechanical properties of the mats

Figure 2a illustrates the mechanical response of the nanofiber mats in the tensile tests. All specimens exhibited a similar profile, with an initial linear region in the stress vs elongational strain plot (i.e., an essentially elastic response), followed by an extensive plastic region with a continuously decreasing slope. Once the maximum strain at failure was reached, the specimens broke with a sudden decrease in stress. Figure 2b shows the Young's modulus, maximum stress and tensile strain at break as calculated from the plot. As can be seen, the three mechanical parameters increased with decreasing SCG:PETbot weight ratio in the nanofibers. The Young's modulus of nanofiber mats increased from 5.1 to 32.8 MPa as SGC:PETbot weight ratio decreased from 2:1 to 0:1, whereas the strain at break and maximum stress values ranged from 13.8 to 39.4% and from 6.6 to 33.1 MPa, respectively. The enhanced mechanical properties of nanofiber mats as PETbot content increased was to be expected for two reasons, namely: (*a*) the nature of PET, which is a linear thermoplastic polymer with excellent mechanical performance (Owen et al., 2023) as compared with lignocellulosic polymers (Akato et al., 2019; Xu et al., 2020); and (*b*) the architectural properties of the electrospun nanofibers (Dodero et al., 2020), which, as stated above, were increasingly uniform, bead-free and thicker as the PETbot proportion was increased. In particular, the average fiber diameter strongly influences the extensional properties of the mats. Thus, both Young's modulus and strain at break linearly correlated with fiber diameter, as shown in Figs. 2c and 2d.

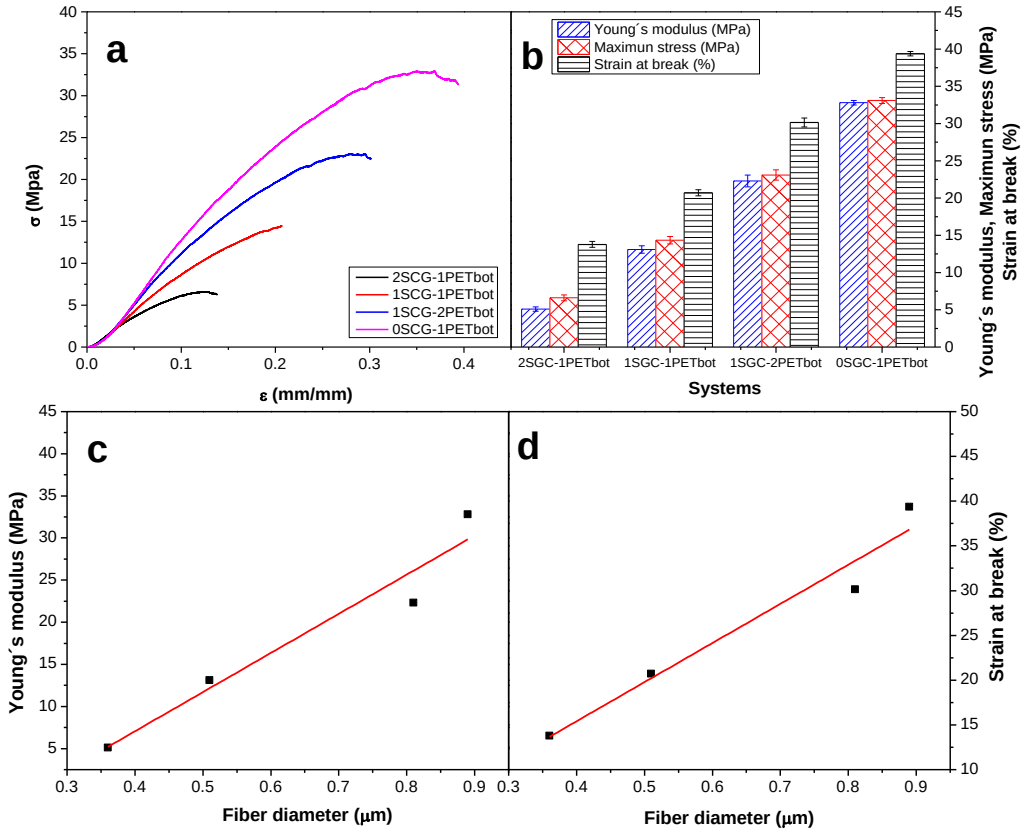

Figure 2. (a) Tensile stress vs elongational strain plots and (b) Young's modulus, maximum stress and tensile strain at break, of SGCs/PETbot electrospun nanostructures differing in SGC:PETbot weight ratio. Linear correlations (R^2 > 0.932) of Young's modulus (c) and strain at break (d) with average nanofiber diameter.

353

354 *3.4. Oil structuring capability of electrospun SGC/PETbot nanofibers*

355 Recent studies have shown that lignin nanostructures consisting largely of
356 electrosprayed particles (i.e., nonfibrous nanostructures) give physically unstable
357 dispersions in vegetable oils (Borrego et al., 2022; Rubio-Valle et al., 2023, 2021),
358 whereas electrospun (bead-free or even slightly beaded) nanofibers can generate
359 physically stable oleogels by forming percolation networks through enhanced physical
360 interactions arising from the high specific surface area and aspect ratio of the
361 nanofibers. The electrospun SCG/PETbot nanofiber mats obtained from the waste
362 materials used here dispersed easily in castor oil to form gel-like dispersions visually
363 resembling those of lubricating greases or oil based coating precursors (Borrero-López
364 et al., 2021; Gallego et al., 2015b). Figure 3 shows the SEM morphology of the oleogel

365 microstructures obtained by dispersing 5 wt.% electrospun SCG/PETbot nanofibers in
366 castor oil. As can be observed, the oleogels obtained with nanofiber webs consisting of
367 2:1 SGC:PETbot (w/w) exhibited a more heterogeneous microstructure and less
368 uniform distribution of fiber diameters than did those obtained with lower SGC:PETbot
369 weight ratios. Upon dispersion in castor oil, the nanofibers agglomerated and swelled to
370 an increasing extent with increasing SGC:PETbot weight ratio. Table 2 shows the
371 degree of nanofiber swelling as calculated from the average diameters obtained from
372 SEM images of electrospun nanofiber networks (Fig. 1) and oleogel microstructures
373 (Fig. 3), and defined as (Rubio-Valle et al., 2023):

374 $$\beta = \frac{Df - D0}{Df}\ x\ 100 \qquad (1)$$

375 where D_o denotes the average diameter of electrospun nanofibers and D_f that of the
376 fibers upon dispersion in the oil medium. As can be seen, the degree of swelling (i.e.,
377 the fiber diameter of the percolation network) increased markedly with increasing
378 SGC:PETbot weight ratio (up to 92% with 2:1), but remained essentially unchanged in
379 SCG-free PETbot nanofibers. Therefore, diffusion of the vegetable oil into nanofibers
380 and the associated swelling occurred mostly in SCG biopolymers (Onwuka et al., 2018,
381 2016). Since castor oil is relatively polar, these results can be ascribed to the
382 hydrophilicity of SCG biopolymers facilitating penetration of triglycerides present in
383 the oil into the fibers and subsequent H-bonding (Boey et al., 2022). This cannot have
384 been the case with PETbot owing to its hydrophobicity (Jasmee et al., 2018; Shukla et
385 al., 2009).

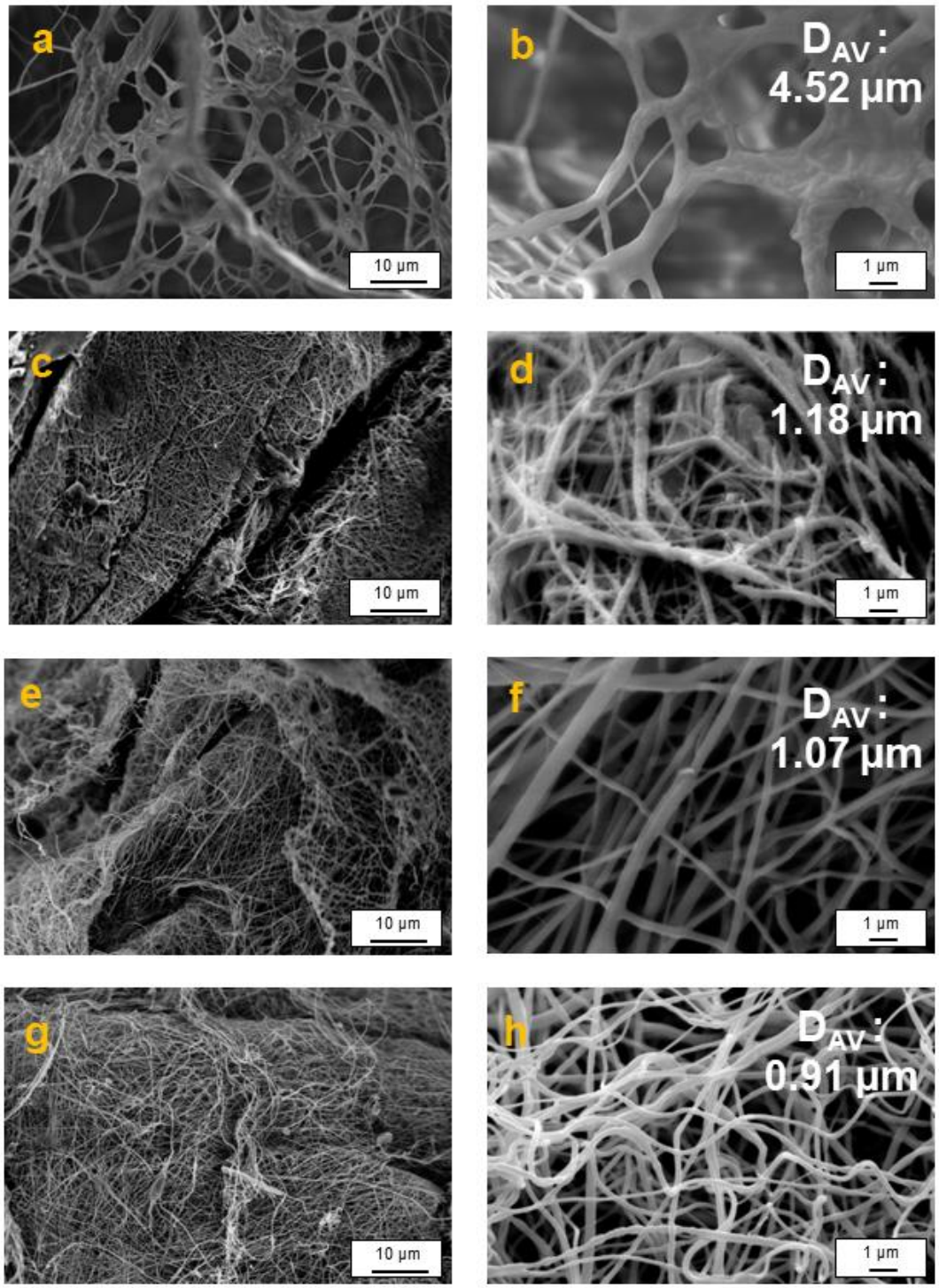

Figure 3. SEM morphological observations of oleogels prepared with electrospun SGC:PETbot nanostructures as a function of the SGC:PETbot weight ratio. (a), (b) O-2SGC-1PETbot. (c), (d) O-1SGC-1 PETbot. (e), (f) O-1SGC-2PETbot. (g), (h) O-0SGCs-1PETbot. Magnification: × 1000 magnification (left), × 10 000 (right).

386

387

Table 2. Swelling factor (eq. 1), and consistency and flow index, for oleogels prepared with electrospun SCG/ PETbot nanostructures, as well as friction coefficient values and wear scar diameters obtained by using the oleogels as lubricants in a ball-on-plates tribological contact

Oleogel	**Swelling factor β (%)**	***K*** **(Pa·s^n)**	***n*** **(−)**	**Friction coefficient (−)**	**Wear scar diameter (μm)**
O-2SGC-1PETbot	92.03^{a}	45.57^{A}	0.14^{aA}	0.165$^{\alpha}$	421 $^{\alpha\alpha}$
O-1SGC-1PETbot	56.78^{b}	98.31^{B}	0.09^{bB}	0.145$^{\beta}$	365 $^{\beta\beta}$
O-1SGC-2PETbot	24.29^{c}	190.89^{C}	0.13^{aA}	0.117$^{\gamma}$	335 $^{\gamma\gamma}$
O-0SGC-1PETbot	2.19^{d}	717.36^{D}	0.06^{bB}	0.092 $^{\gamma}$	315 $^{\gamma\gamma}$
Commercial NLGI 2 lithium grease *	-	-	-	0.113	273
Commercial NLGI 2 calcium grease *	-	-	-	0.112	321

Values on the same column differing in their superscripts were significantly different ($p < 0.05$)
* data taken from Gallego et al. (2016)

388

389 Figures 4a−4c show the variation of the SAOS functions (viz., the storage modulus, G',
390 the loss modulus, G'' , and the loss tangent, G''/G') with frequency in the oleogels
391 obtained by dispersing 5 wt% electrospun SCG/PETbot nanofiber mats in castor oil at
392 variable SCG:PETbot ratios. As can be seen, all samples gave very similar mechanical
393 spectra typical of gel-like dispersions that differed only in the magnitude of G' and G''
394 —which increased by almost two decades with decreasing SCG:PETbot ratio. On the
395 other hand, the loss tangent, indicative of the relative elastic character, differed little but
396 was slightly lower in nanofibers consisting mainly of PETbot (1:2 and 0:1 SCG:PETbot
397 ratios), especially at high frequencies (see Fig. 4c). This viscoelastic behavior
398 corresponds to the so-called plateau zone of the SAOS functions vs. frequency plots,
399 where G' exceeds G'' over an extended frequency range and is almost independent of
400 the frequency whereas G'' tends to a minimum. An extended plateau region of the
401 mechanical spectrum is typical of physical entanglement in polymeric materials (Ferry,
402 1980) and, in our case, reflects the packing effect of the percolation network formed by

electrospun fibers. A very similar rheological response is exhibited by conventional lubricating greases, with typical G' values of 10^3–10^5 Pa depending on the thickener type and concentration, and G'' values roughly one order of magnitude lower (Sánchez et al., 2014). This mechanical spectrum is characterized in rheological terms by the plateau modulus (G_N^0), which is a measure of entanglement density and hence of gel strength (Baurngaertel et al., 1992). The observed increase in gel strength with decreasing SCG:PETbot ratio can be ascribed to the intrinsic mechanical properties of the nanofiber mats (specifically, to their Young's modulus). As can be seen in Fig. 4e, the plateau modulus (G_N^0) of the oleogels increased exponentially —linearly on a log scale— with increasing Young's modulus in the electrospun nanofiber mats, which in turn correlated with the average nanofiber diameter (see Fig.2c).

Regarding the viscous flow response, Fig. 4d shows the viscosity vs. shear rate plots for oleogels prepared with electrospun nanofibers differing in SCG:PETbot ratio. A shear-thinning behavior was invariably observed over the experimental shear rate range studied that fitted the power-law model:

$$\eta = K \cdot \dot{\gamma}^{\,n-1} \tag{2}$$

where K and n are the consistency and flow indices, respectively. Table 2 shows the K and n values obtained by fitting the data to eq. (2). Similarly to SAOS functions, the lower was the SCG:PETbot weight ratio of the nanofiber mats, the higher was K. However, the low values of the flow index, n, reveal strong shear-thinning responses in all cases. As previously shown for G_N^0, K was also exponentially correlated with Young's modulus in the nanofiber mats. Overall, the morphology and mechanical properties of the electrospun nanoarchitectures governed the rheological properties of the oleogels and can be tuned through the SCG:PETbot ratio. It should be noted that the rheological response of oleogels containing only 5 wt.% nanofibers was comparable to that of conventional lubricating greases with much higher thickener contents (e.g., lithium soaps; Delgado et al., 2006).

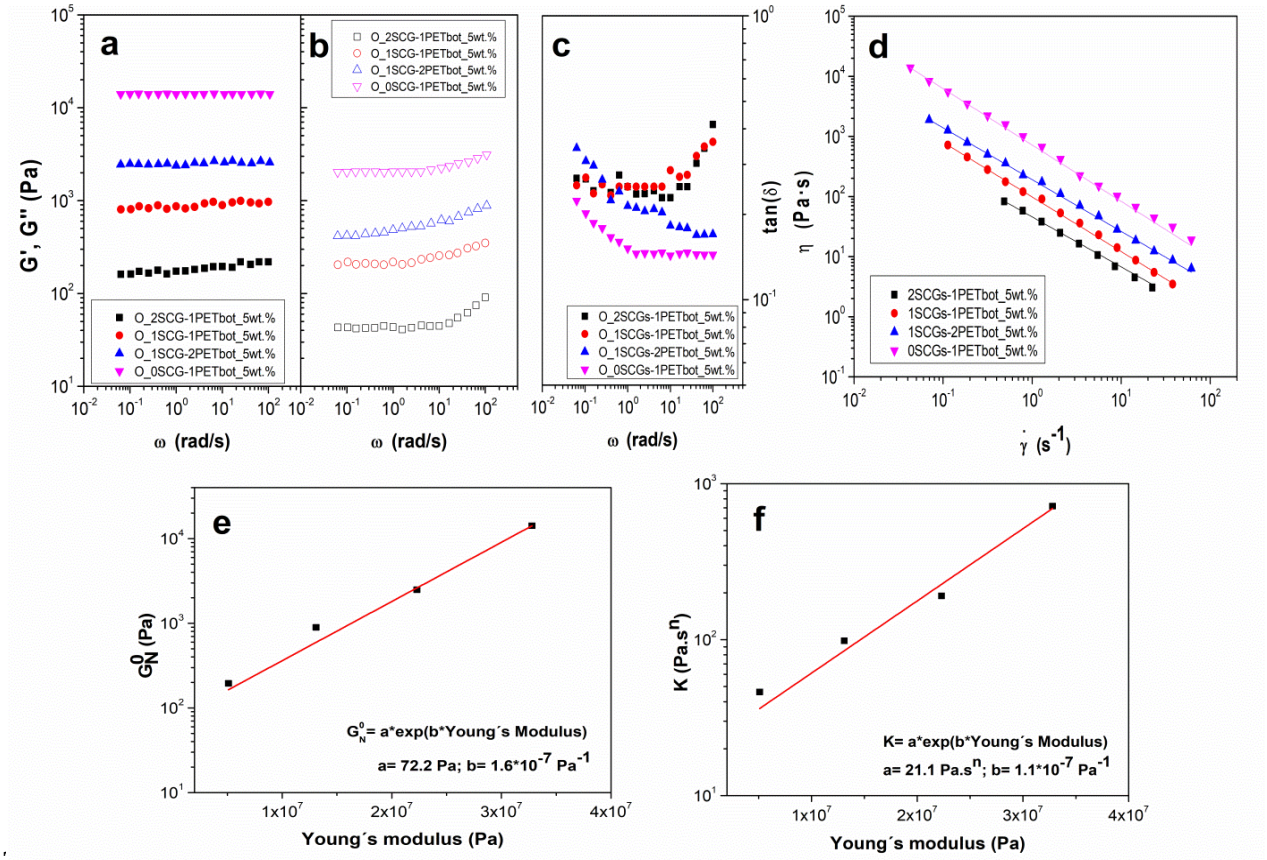

Figure 4. Influence of the SCG:PETbot weight ratio and the mechanical properties of the associated nanostructure on the rheological properties of the oleogels. Variation of (a) storage modulus (G'), (b) loss modulus (G'') and (c) loss tangent with frequency; (d) variation of viscosity with shear rate, and correlations ($R^2 > 0.981$) of (e) the plateau modulus and (f) the consistency index of the oleogels with Young's modulus for the nanofiber mats.

3.5. Lubrication performance of the oleogels

Bearing in mind the potential use as lubricants of the oleogels, their lubrication performance was assessed by measuring friction and wear scar in a tribological steel−steel contact. For this purpose, friction coefficients were recorded at constant normal load (20 N) and rotational speed (10 rpm) over time. Their average values are shown in Table 2 together with the average diameter of the wear marks generated on the plates upon completion of the friction test. As can be seen, both friction and wear dimensions were significantly reduced by mats with increased PETbot contents. As stated above, this was the likely result of nanofibers with increased PETbot ratios being much less prone to swelling in the oleogel, thus allowing the oil to be released more easily into the lubricated contact. In addition, the higher viscosity of oleogels prepared

with nanofibers of lower SCG:PETbot ratios (see Fig. 4d) must favour the increase of the lubricant film thickness thus preventing friction and wear.

On the other hand, most of the oleogels exhibited acceptable friction coefficients and antiwear performance when used as lubricants, comparable to those found with commercial lubricating greases (Gallego et al., 2016; Zhang et al., 2018) and other oleogels produced with chemically modified biopolymers (Cortés-Triviño et al., 2019) under similar conditions. For the sake of comparison, Table 2 also shows friction coefficient and wear diameter data (Gallego et al., 2016) obtained when using conventional NLGI 2 lithium and calcium greases as lubricants, tested in the same tribological cell under identical conditions as the oleogels. As can be observed, the friction coefficient values measured with oleogels prepared with nanofiber mats of low SCG:PETbot ratios (1:2 and 0:1) were similar to or even lower than those found with these commercial greases. Regarding wear marks, most of the SCG/PETbot nanofibers-based oleogels provided a wear prevention functionality comparable to that shown by the calcium grease.

3.6. Outlook

3.6.1. Limitations and further work

This work demonstrates that the methodology used to obtain nanofibers with the ability to structure oil from waste materials such as SCG and PETbot is effective and relatively simple, and avoids any chemical modification of the structuring agent to enhance the compatibility with oil. However, this methodology is not without limitations and future work should be directed towards overcoming these. One of the main drawbacks of electrospinning to be implemented at a large scale is its low production efficiency due to the usually low feeding rate and possible nozzle clogging. Certainly, nowadays there are a number of alternatives available based on multiple needles in parallel and needle-less arrangements that allow an affordable scale-up of this technology (Hernandez et al., 2022; Shi and Giapis, 2018; Xu et al., 2023). Nevertheless, these configurations can improve efficiency to a certain extent but still cause some other problems such as multi-

needle electric field interference, generation of inhomogeneous fibers, and/or poor fiber distribution in the collector (Xue et al., 2019), while for needle-less electrospinning the stability of the electrospun jet and controllability of the equipment are far lower than that of needle-based electrospinning equipments (Si et al., 2023). Therefore, scale-up tests need to be performed to assess the efficiency and effectiveness of this technology to produce SCG/PETbot nanofibers at a large scale. On the other hand, the proposed methodology consists of a two-step oleogel manufacturing process, firstly obtaining the nanofiber mats and, subsequently, the efficient dispersion in the oily medium. From a cost-efficiency point of view, the integration of the two steps in a single operation is a challenge that should be addressed, for example by designing a collector system in the electrospinning chamber that includes the direct incorporation of the nanofibers into the oil.

The other main limitation of this methodology is the use of harmful solvents such as TFA to dissolve SCG and feed the electrospinning chamber. SCG as a complex lignocellulosic waste material is difficult to dissolve. In this respect, there is still much room for improvement in the search for environmentally friendly solvents suitable for these hard-to-dissolve lignocellulosic materials that can also be easily electrospinnable. In this sense, alternatives such as ionic liquids and NADES could be envisaged.

Finally, a more exhaustive tribological and thermo-rheological characterization of the oleogels prepared with electrospun SCG/PETbot nanofibers should be performed to ensure a proper implementation as lubricants.

3.6.2. Contribution to the sustainable development

Despite the aforementioned limitations, this work explores for the first time the use of spent coffee grounds (SCG) and post-consumer bottles (PETbot) to obtain electrospun nanofiber mats with a view to valorizing or upcycling these environmentally relevant waste materials in high added-value applications which require oil structuring. As mentioned in the Introduction section, the finding of suitable environmentally friendly, renewable and/or recycled oil structuring and thickening agents is challenging for

several industrial sectors. For instance, the proposed approach could provide a new niche market for some industrial sectors such as lubricant and coating production, where a pressing need exists to replace conventional thickening agents for oils. Moreover, the use of these kinds of waste materials as structuring agents is likely to yield more cost-effective formulations than those based on metal soaps and polyureas.

Therefore, upcycling SCG and PETbot into nanofiber mats for oil structuring applications is fully aligned with the UN Sustainable Development Goals (SDG), and more specifically with the 12th SDG related to "Response Consumption and Production" which clearly establishes targets such as substantially reducing waste generation through prevention, reduction, recycling and reuse; achieving the environmentally sound management of chemicals and all wastes throughout their life cycle; or strengthening the scientific and technological capacity to move towards more sustainable consumption and production patterns.

4. Conclusions

From the experimental results, the following conclusions can be derived:

- Electrospinning SCG solutions did not generate nanofibers but microsized electrosprayed particles. However, adding PETbot as a cospinning polymer provided homogeneous nanofiber networks with some beaded nanofibers. Increasing the PETbot:SCG weight ratio above 1:1 prevented the formation of beads and increased the average fiber diameter. As a result, the tensile properties of the nanofiber mats improved with increasing proportion of PETbot in the nanofibers.
- Dispersions of electrospun SCG/PETbot nanofibers in castor oil exhibited gel-like viscoelastic responses and shear-thinning characteristics comparable with those of conventional lubricating greases, and also tribological properties suitable for their use as lubricants.
- The rheological properties of the oleogels depend on the morphology and mechanical properties of the electrospun SCG/PETbot nanofiber mats. Linear viscoelastic functions, relative elasticity and shear viscosity increased with increasing proportion

of PETbot in the mats. The plateau modulus and the consistency index of the oleogels correlated exponentially with Young's modulus in the mats.

- Overall, SCG and PETbot can be used to obtain electrospun nanofiber mats with oil structuring capabilities. The resulting oleogels can be used as environmentally friendly alternatives to conventional lubricating greases and their rheological properties tuned through the SCG:PETbot weight ratio.

Acknowledgements

This study has been carried out in the framework of the Research Project PID2021-125637OB-I00, funded by MCIN/AEI/10.13039/501100011033 and by "ERDF A way of making Europe". J.F. Rubio-Valle additionally received a PhD Research Grant PRE2019-090632 from Spain's Ministry of Science and Innovation. Funding for open access charge: Universidad de Huelva / CBUA. All funding is gratefully acknowledged.

References

Akato, K.M., Nguyen, N.A., Rajan, K., Harper, D.P., Naskar, A.K., 2019. A tough and sustainable fiber-forming material from lignin and waste poly(ethylene terephthalate). RSC Adv. 9, 31202–31211. https://doi.org/10.1039/C9RA07052D

Baker, D.A., Rials, T.G., 2013. Recent advances in low-cost carbon fiber manufacture from lignin. J. Appl. Polym. Sci. 130, 713–728. https://doi.org/10.1002/app.39273

Bashir, Z., Yu, W., Xu, Z., Li, Yiran, Lai, J., Li, Ying, Cao, Y., Xue, B., 2022. Engineering Bio-Adhesives Based on Protein–Polysaccharide Phase Separation. Int. J. Mol. Sci. 23, 9987. https://doi.org/10.3390/ijms23179987

Baurngaertel, M., De Rosa, M.E., Machado, J., Masse, M., Winter, H.H., 1992. The relaxation time spectrum of nearly monodisperse polybutadiene melts. Rheol. Acta 31, 75–82. https://doi.org/10.1007/BF00396469

Boey, J.Y., Yusoff, S.B., Tay, G.S., 2022. A review on the enhancement of composite's

564 interface properties through biological treatment of natural fibre/lignocellulosic
565 material. Polym. Polym. Compos. 30, 096739112211036.
566 https://doi.org/10.1177/09673911221103600
567 Bomfim, A., Oliveira, D., Voorwald, H., Benini, K., Dumont, M.-J., Rodrigue, D.,
568 2022. Valorization of Spent Coffee Grounds as Precursors for Biopolymers and
569 Composite Production. Polymers (Basel). 14, 437.
570 https://doi.org/10.3390/polym14030437
571 Borrego, M., Martín-Alfonso, J.E., Sánchez, M.C., Valencia, C., Franco, J.M., 2021.
572 Electrospun lignin-PVP nanofibers and their ability for structuring oil. Int. J. Biol.
573 Macromol. 180, 212–221. https://doi.org/10.1016/j.ijbiomac.2021.03.069
574 Borrego, M., Martín-Alfonso, J.E., Valencia, C., Sánchez Carrillo, M. del C., Franco,
575 J.M., 2022. Developing Electrospun Ethylcellulose Nanofibrous Webs: An
576 Alternative Approach for Structuring Castor Oil. ACS Appl. Polym. Mater. 4,
577 7217–7227. https://doi.org/10.1021/acsapm.2c01090
578 Borrero-López, A.M., Blánquez, A., Valencia, C., Hernández, M., Arias, M.E.,
579 Eugenio, M.E., Fillat, Ú., Franco, J.M., 2018. Valorization of Soda Lignin from
580 Wheat Straw Solid-State Fermentation: Production of Oleogels. ACS Sustain.
581 Chem. Eng. 6, 5198–5205. https://doi.org/10.1021/acssuschemeng.7b04846
582 Borrero-López, A.M., Valencia, C., Domínguez, G., Eugenio, M.E., Franco, J.M., 2021.
583 Rheology and adhesion performance of adhesives formulated with lignins from
584 agricultural waste straws subjected to solid-state fermentation. Ind. Crops Prod.
585 171, 113876. https://doi.org/10.1016/j.indcrop.2021.113876
586 Borrero-López, A.M., Valencia, C., Franco, J.M., 2017. Rheology of lignin-based
587 chemical oleogels prepared using diisocyanate crosslinkers: Effect of the
588 diisocyanate and curing kinetics. Eur. Polym. J. 89, 311–323.

https://doi.org/10.1016/j.eurpolymj.2017.02.020

Brachi, P., Santes, V., Torres-Garcia, E., 2021. Pyrolytic degradation of spent coffee ground: A thermokinetic analysis through the dependence of activation energy on conversion and temperature. Fuel 302, 120995. https://doi.org/10.1016/j.fuel.2021.120995

Camacho-Otero, J., Boks, C., Pettersen, I., 2018. Consumption in the Circular Economy: A Literature Review. Sustainability 10, 2758. https://doi.org/10.3390/su10082758

Campos-Vega, R., Loarca-Piña, G., Vergara-Castañeda, H.A., Oomah, B.D., 2015. Spent coffee grounds: A review on current research and future prospects. Trends Food Sci. Technol. 45, 24–36. https://doi.org/10.1016/j.tifs.2015.04.012

Cheng, Q.-Y., Liu, M.-C., Li, Y.-D., Zhu, J., Du, A.-K., Zeng, J.-B., 2018. Biobased super-hydrophobic coating on cotton fabric fabricated by spray-coating for efficient oil/water separation. Polym. Test. 66, 41–47. https://doi.org/10.1016/j.polymertesting.2018.01.005

Cortés-Triviño, E., Valencia, C., Delgado, M.A., Franco, J.M., 2019. Thermo-rheological and tribological properties of novel bio-lubricating greases thickened with epoxidized lignocellulosic materials. J. Ind. Eng. Chem. 80, 626–632. https://doi.org/10.1016/j.jiec.2019.08.052

Cortés-Triviño, E., Valencia, C., Delgado, M.A., Franco, J.M., 2018. Rheology of epoxidized cellulose pulp gel-like dispersions in castor oil: Influence of epoxidation degree and the epoxide chemical structure. Carbohydr. Polym. 199, 563–571. https://doi.org/10.1016/j.carbpol.2018.07.058

Cortés-Triviño, E., Valencia, C., Franco, J.M., 2021. Thickening Castor Oil with a Lignin-Enriched Fraction from Sugarcane Bagasse Waste via Epoxidation: A

614 Rheological and Hydrodynamic Approach. ACS Sustain. Chem. Eng. 9, 10503–
615 10512. https://doi.org/10.1021/acssuschemeng.1c02166
616 Dallmeyer, I., Ko, F., Kadla, J.F., 2010. Electrospinning of Technical Lignins for the
617 Production of Fibrous Networks. J. Wood Chem. Technol. 30, 315–329.
618 https://doi.org/10.1080/02773813.2010.527782
619 Dallmeyer, I., Lin, L.T., Li, Y., Ko, F., Kadla, J.F., 2014. Preparation and
620 Characterization of Interconnected, Kraft Lignin-Based Carbon Fibrous Materials
621 by Electrospinning. Macromol. Mater. Eng. 299, 540–551.
622 https://doi.org/10.1002/mame.201300148
623 Das, P., Tiwari, P., 2019. Thermal degradation study of waste polyethylene
624 terephthalate (PET) under inert and oxidative environments. Thermochim. Acta
625 679, 178340. https://doi.org/10.1016/j.tca.2019.178340
626 Davidovich-Pinhas, M., 2016. Oleogels: a promising tool for delivery of hydrophobic
627 bioactive molecules. Ther. Deliv. 7, 1–3. https://doi.org/10.4155/tde.15.83
628 Davila-Guzman, N.E., Cerino-Córdova, F.J., Loredo-Cancino, M., Rangel-Mendez,
629 J.R., Gómez-González, R., Soto-Regalado, E., 2016. Studies of Adsorption of
630 Heavy Metals onto Spent Coffee Ground: Equilibrium, Regeneration, and
631 Dynamic Performance in a Fixed-Bed Column. Int. J. Chem. Eng. 2016, 1–11.
632 https://doi.org/10.1155/2016/9413879
633 Delgado, M.A., Valencia, C., Sánchez, M.C., Franco, J.M., Gallegos, C., 2006.
634 Influence of Soap Concentration and Oil Viscosity on the Rheology and
635 Microstructure of Lubricating Greases. Ind. Eng. Chem. Res. 45, 1902–1910.
636 https://doi.org/10.1021/ie050826f
637 Dericiler, K., Kocanali, A., Buldu-Akturk, M., Erdem, E., Saner Okan, B., 2022.
638 Upcycling process of transforming waste coffee into spherical graphene by flash

639 pyrolysis for sustainable supercapacitor manufacturing with virgin graphene
640 electrodes and its comparative life cycle assessment. Biomass Convers.
641 Biorefinery. https://doi.org/10.1007/s13399-022-02447-8
642 Dodero, A., Brunengo, E., Castellano, M., Vicini, S., 2020. Investigation of the
643 Mechanical and Dynamic-Mechanical Properties of Electrospun
644 Polyvinylpyrrolidone Membranes: A Design of Experiment Approach. Polymers
645 (Basel). 12, 1524. https://doi.org/10.3390/polym12071524
646 Evode, N., Qamar, S.A., Bilal, M., Barceló, D., Iqbal, H.M.N., 2021. Plastic waste and
647 its management strategies for environmental sustainability. Case Stud. Chem.
648 Environ. Eng. 4, 100142. https://doi.org/10.1016/j.cscee.2021.100142
649 Ferry, J.D., 1980. Viscoelastic properties of polymers, 3rd ed., Wiley, New York.
650 Forcina, A., Petrillo, A., Travaglioni, M., di Chiara, S., De Felice, F., 2023. A
651 comparative life cycle assessment of different spent coffee ground reuse strategies
652 and a sensitivity analysis for verifying the environmental convenience based on the
653 location of sites. J. Clean. Prod. 385, 135727.
654 https://doi.org/10.1016/j.jclepro.2022.135727
655 Franca, A.S., Oliveira, L.S., 2022. Potential Uses of Spent Coffee Grounds in the Food
656 Industry. Foods 11, 2064. https://doi.org/10.3390/foods11142064
657 Gallego, R., Arteaga, J.F., Valencia, C., Díaz, M.J., Franco, J.M., 2015a. Gel-Like
658 Dispersions of HMDI-Cross-Linked Lignocellulosic Materials in Castor Oil:
659 Toward Completely Renewable Lubricating Grease Formulations. ACS Sustain.
660 Chem. Eng. 3, 2130–2141. https://doi.org/10.1021/acssuschemeng.5b00389
661 Gallego, R., Arteaga, J.F., Valencia, C., Franco, J.M., 2015b. Thickening properties of
662 several NCO-functionalized cellulose derivatives in castor oil. Chem. Eng. Sci.
663 134, 260–268. https://doi.org/10.1016/j.ces.2015.05.007

Gallego, R., Arteaga, J.F., Valencia, C., Franco, J.M., 2013. Rheology and thermal degradation of isocyanate-functionalized methyl cellulose-based oleogels. Carbohydr. Polym. 98, 152–160. https://doi.org/10.1016/j.carbpol.2013.04.104

Gallego, R., Cidade, T., Sánchez, R., Valencia, C., Franco, J.M., 2016. Tribological behaviour of novel chemically modified biopolymer-thickened lubricating greases investigated in a steel–steel rotating ball-on-three plates tribology cell. Tribol. Int. 94, 652–660. https://doi.org/10.1016/j.triboint.2015.10.028

Geisendorf, S., Pietrulla, F., 2018. The circular economy and circular economic concepts-a literature analysis and redefinition. Thunderbird Int. Bus. Rev. 60, 771–782. https://doi.org/10.1002/tie.21924

Gupta, A., Mohanty, A.K., Misra, M., 2022. Biocarbon from spent coffee ground and their sustainable biocomposites with recycled water bottle and bale wrap: A new life for waste plastics and waste food residues for industrial uses. Compos. Part A Appl. Sci. Manuf. 154, 106759. https://doi.org/10.1016/j.compositesa.2021.106759

Hernandez, J.L., Doan, M.-A., Stoddard, R., VanBenschoten, H.M., Chien, S.-T., Suydam, I.T., Woodrow, K.A., 2022. Scalable Electrospinning Methods to Produce High Basis Weight and Uniform Drug Eluting Fibrous Biomaterials. Front. Biomater. Sci. 1. https://doi.org/10.3389/fbiom.2022.928537

Heyer, P., Läuger, J., 2009. Correlation between friction and flow of lubricating greases in a new tribometer device. Lubr. Sci. 21, 253–268. https://doi.org/10.1002/ls.88

Hossain, M.T., Shahid, M.A., Ali, A., 2022. Development of nanofibrous membrane from recycled polyethene terephthalate bottle by electrospinning. OpenNano 8, 100089. https://doi.org/10.1016/j.onano.2022.100089

Jasmee, S., Omar, G., Masripan, N.A.B., Kamarolzaman, A.A., Ashikin, A.S., Che Ani, F., 2018. Hydrophobicity performance of polyethylene terephthalate (PET) and

thermoplastic polyurethane (TPU) with thermal effect. Mater. Res. Express 5, 096304. https://doi.org/10.1088/2053-1591/aad81e

Jin Ong, P., Leow, Y., Yun Debbie Soo, X., Hui Chua, M., Ni, X., Suwardi, A., Kiang Ivan Tan, C., Zheng, R., Wei, F., Xu, J., Jun Loh, X., Kai, D., Zhu, Q., 2023. Valorization of Spent coffee Grounds: A sustainable resource for Bio-based phase change materials for thermal energy storage. Waste Manag. 157, 339–347. https://doi.org/10.1016/j.wasman.2022.12.039

Kang, B.-J., Jeon, J.-M., Bhatia, S.K., Kim, D.-H., Yang, Y.-H., Jung, S., Yoon, J.-J., 2023. Two-Stage Bio-Hydrogen and Polyhydroxyalkanoate Production: Upcycling of Spent Coffee Grounds. Polymers (Basel). 15, 681. https://doi.org/10.3390/polym15030681

Kasbaji, M., Mennani, M., Grimi, N., Oubenali, M., Mbarki, M., EL Zakhem, H., Moubarik, A., 2023. Adsorption of cationic and anionic dyes onto coffee grounds cellulose/sodium alginate double-network hydrogel beads: Isotherm analysis and recyclability performance. Int. J. Biol. Macromol. 239, 124288. https://doi.org/10.1016/j.ijbiomac.2023.124288

Leow, Y., Yew, P.Y.M., Chee, P.L., Loh, X.J., Kai, D., 2021. Recycling of spent coffee grounds for useful extracts and green composites. RSC Adv. 11, 2682–2692. https://doi.org/10.1039/D0RA09379C

Lubesn Greases, 2021. No Title. https://www.lubesngreases.com/magazine/27_4/grease-holds-promise-for-evolving-industry/.

Michelini, G., Moraes, R.N., Cunha, R.N., Costa, J.M.H., Ometto, A.R., 2017. From Linear to Circular Economy: PSS Conducting the Transition. Procedia CIRP 64, 2–6. https://doi.org/10.1016/j.procir.2017.03.012

714 Morseletto, P., 2020. Targets for a circular economy. Resour. Conserv. Recycl. 153,
715 104553. https://doi.org/10.1016/j.resconrec.2019.104553
716 Naderi Kalali, E., Lotfian, S., Entezar Shabestari, M., Khayatzadeh, S., Zhao, C.,
717 Yazdani Nezhad, H., 2023. A critical review of the current progress of plastic
718 waste recycling technology in structural materials. Curr. Opin. Green Sustain.
719 Chem. 100763. https://doi.org/10.1016/j.cogsc.2023.100763
720 Nanni, A., Colonna, M., Messori, M., 2022. Fabrication and characterization of new
721 eco-friendly composites obtained by the complete recycling of exhausted coffee
722 capsules. Compos. Sci. Technol. 222, 109358.
723 https://doi.org/10.1016/j.compscitech.2022.109358
724 Ncube, L.K., Ude, A.U., Ogunmuyiwa, E.N., Zulkifli, R., Beas, I.N., 2021. An
725 Overview of Plastic Waste Generation and Management in Food Packaging
726 Industries. Recycling 6, 12. https://doi.org/10.3390/recycling6010012
727 Nieva, A.D., Buenafe, R.J.Q., Guinto, D.R., Leaño, J.C.F., 2019. Biosorption of Copper
728 (II) from Simulated Wastewater Using Spent Coffee Grounds: A Column Study.
729 Int. J. Environ. Sci. Dev. 10, 261–265.
730 https://doi.org/10.18178/ijesd.2019.10.9.1184
731 Onwuka, J.C., Agbaji, E.B., Ajibola, V.O., Okibe, F.G., 2018. Treatment of crude oil-
732 contaminated water with chemically modified natural fiber. Appl. Water Sci. 8, 86.
733 https://doi.org/10.1007/s13201-018-0727-5
734 Onwuka, J.C., Agbaji, E.B., Ajibola, V.O., Okibe, F.G., 2016. Kinetic studies of surface
735 modification of lignocellulosic Delonix regia pods as sorbent for crude oil spill in
736 water. J. Appl. Res. Technol. 14, 415–424.
737 https://doi.org/10.1016/j.jart.2016.09.004
738 Owen, M.M., Achukwu, E.O., Romli, A.Z., Md Akil, H., 2023. Recent advances on

improving the mechanical and thermal properties of kenaf fibers/engineering thermoplastic composites using novel coating techniques: a review. Compos. Interfaces 1–27. https://doi.org/10.1080/09276440.2023.2179238

Pagett, M., Teng, K.S., Sullivan, G., Zhang, W., 2023. Reusing Waste Coffee Grounds as Electrode Materials: Recent Advances and Future Opportunities. Glob. Challenges 7, 2200093. https://doi.org/10.1002/gch2.202200093

Pakseresht, S., Mazaheri Tehrani, M., 2022. Advances in Multi-component Supramolecular Oleogels- a Review. Food Rev. Int. 38, 760–782. https://doi.org/10.1080/87559129.2020.1742153

Panchal, T.M., Patel, A., Chauhan, D.D., Thomas, M., Patel, J. V., 2017. A methodological review on bio-lubricants from vegetable oil based resources. Renew. Sustain. Energy Rev. 70, 65–70. https://doi.org/10.1016/j.rser.2016.11.105

Patel, A.R., 2018. Structuring Edible Oils with Hydrocolloids: Where Do we Stand? Food Biophys. 13, 113–115. https://doi.org/10.1007/s11483-018-9527-6

Patel, A.R., 2017. A colloidal gel perspective for understanding oleogelation. Curr. Opin. Food Sci. 15, 1–7. https://doi.org/10.1016/j.cofs.2017.02.013

Pathan, A.K., Bond, J., Gaskin, R.E., 2010. Sample preparation for SEM of plant surfaces. Mater. Today 12, 32–43. https://doi.org/10.1016/S1369-7021(10)70143-7

Pereira, A.P. dos S., Silva, M.H.P. da, Lima Júnior, É.P., Paula, A. dos S., Tommasini, F.J., 2017. Processing and Characterization of PET Composites Reinforced With Geopolymer Concrete Waste. Mater. Res. 20, 411–420. https://doi.org/10.1590/1980-5373-mr-2017-0734

Quinchia, L.A., Delgado, M.A., Valencia, C., Franco, J.M., Gallegos, C., 2010. Viscosity modification of different vegetable oils with EVA copolymer for lubricant applications. Ind. Crops Prod. 32, 607–612.

https://doi.org/10.1016/j.indcrop.2010.07.011

Raghunanan, L.C., Fernandez-Prieto, S., Martínez, I., Valencia, C., Sánchez, M.C., Franco, J.M., 2018. Molecular insights into the mechanisms of humidity-induced changes on the bulk performance of model castor oil derived polyurethane adhesives. Eur. Polym. J. 101, 291–303. https://doi.org/10.1016/j.eurpolymj.2018.02.041

Rahmati Nejad, M., Yousefzadeh, M., Solouk, A., 2020. Electrospun PET/PCL small diameter nanofibrous conduit for biomedical application. Mater. Sci. Eng. C 110, 110692. https://doi.org/10.1016/j.msec.2020.110692

Reynolds, C., Geschke, A., Piantadosi, J., Boland, J., 2016. Estimating industrial solid waste and municipal solid waste data at high resolution using economic accounts: an input–output approach with Australian case study. J. Mater. Cycles Waste Manag. 18, 677–686. https://doi.org/10.1007/s10163-015-0363-1

Rosenboom, J.-G., Langer, R., Traverso, G., 2022. Bioplastics for a circular economy. Nat. Rev. Mater. 7, 117–137. https://doi.org/10.1038/s41578-021-00407-8

Rubio-Valle, J.F., Sánchez, M.C., Valencia, C., Martín-Alfonso, J.E., Franco, J.M., 2021. Electrohydrodynamic Processing of PVP-Doped Kraft Lignin Micro- and Nano-Structures and Application of Electrospun Nanofiber Templates to Produce Oleogels. Polymers (Basel). 13, 2206. https://doi.org/10.3390/polym13132206

Rubio-Valle, J.F., Valencia, C., Sánchez, M., Martín-Alfonso, J.E., Franco, J.M., 2023. Oil structuring properties of electrospun Kraft lignin/cellulose acetate nanofibers for lubricating applications: influence of lignin source and lignin/cellulose acetate ratio. Cellulose 30, 1553–1566. https://doi.org/10.1007/s10570-022-04963-2

Sadeghi, B., Marfavi, Y., AliAkbari, R., Kowsari, E., Borbor Ajdari, F., Ramakrishna, S., 2021. Recent Studies on Recycled PET Fibers: Production and Applications: a

789 Review. Mater. Circ. Econ. 3, 4. https://doi.org/10.1007/s42824-020-00014-y
790 Sahoo, S., Mohanty, S., Nayak, S.K., 2018. Biobased polyurethane adhesive over
791 petroleum based adhesive: Use of renewable resource. J. Macromol. Sci. Part A 55,
792 36–48. https://doi.org/10.1080/10601325.2017.1387486
793 Sánchez, R., Valencia, C., Franco, J.M., 2014. Rheological and Tribological
794 Characterization of a New Acylated Chitosan–Based Biodegradable Lubricating
795 Grease: A Comparative Study with Traditional Lithium and Calcium Greases.
796 Tribol. Trans. 57, 445–454. https://doi.org/10.1080/10402004.2014.880541
797 Santos, R.P.O., Rodrigues, B.V.M., Ramires, E.C., Ruvolo-Filho, A.C., Frollini, E.,
798 2015. Bio-based materials from the electrospinning of lignocellulosic sisal fibers
799 and recycled PET. Ind. Crops Prod. 72, 69–76.
800 https://doi.org/10.1016/j.indcrop.2015.01.024
801 Sarja, M., Onkila, T., Mäkelä, M., 2021. A systematic literature review of the transition
802 to the circular economy in business organizations: Obstacles, catalysts and
803 ambivalences. J. Clean. Prod. 286, 125492.
804 https://doi.org/10.1016/j.jclepro.2020.125492
805 Shanmugam, V., Das, O., Neisiany, R.E., Babu, K., Singh, S., Hedenqvist, M.S., Berto,
806 F., Ramakrishna, S., 2020. Polymer Recycling in Additive Manufacturing: an
807 Opportunity for the Circular Economy. Mater. Circ. Econ. 2, 11.
808 https://doi.org/10.1007/s42824-020-00012-0
809 Shi, K., Giapis, K.P., 2018. Scalable Fabrication of Supercapacitors by Nozzle-Free
810 Electrospinning. ACS Appl. Energy Mater. 1, 296–300.
811 https://doi.org/10.1021/acsaem.7b00227
812 Shukla, S.R., Harad, A.M., Jawale, L.S., 2009. Chemical recycling of PET waste into
813 hydrophobic textile dyestuffs. Polym. Degrad. Stab. 94, 604–609.

https://doi.org/10.1016/j.polymdegradstab.2009.01.007

Si, Y., Shi, S., Hu, J., 2023. Applications of electrospinning in human health: From detection, protection, regulation to reconstruction. Nano Today 48, 101723. https://doi.org/10.1016/j.nantod.2022.101723

Smith, R.L., Takkellapati, S., Riegerix, R.C., 2022. Recycling of Plastics in the United States: Plastic Material Flows and Polyethylene Terephthalate (PET) Recycling Processes. ACS Sustain. Chem. Eng. 10, 2084–2096. https://doi.org/10.1021/acssuschemeng.1c06845

Sridhar, A., Kapoor, A., Senthil Kumar, P., Ponnuchamy, M., Balasubramanian, S., Prabhakar, S., 2021. Conversion of food waste to energy: A focus on sustainability and life cycle assessment. Fuel 302, 121069. https://doi.org/10.1016/j.fuel.2021.121069

Statista, 2023. No Title. https://www.statista.com/statistics/282732/global-production-of-plastics-since-1950/.

Stokroos, Kalicharan, Van Der Want, Jongebloed, 1998. A comparative study of thin coatings of Au/Pd, Pt and Cr produced by magnetron sputtering for FE- SEM. J. Microsc. 189, 79–89. https://doi.org/10.1046/j.1365-2818.1998.00282.x

Strain, I.N., Wu, Q., Pourrahimi, A.M., Hedenqvist, M.S., Olsson, R.T., Andersson, R.L., 2015. Electrospinning of recycled PET to generate tough mesomorphic fibre membranes for smoke filtration. J. Mater. Chem. A 3, 1632–1640. https://doi.org/10.1039/C4TA06191H

Svinterikos, E., Zuburtikudis, I., Al-Marzouqi, M., 2020. Fabricating carbon nanofibers from a lignin/r-PET blend: the synergy of mass ratio with the average fiber diameter. Appl. Nanosci. 10, 1331–1343. https://doi.org/10.1007/s13204-019-01235-7

839 Syahir, A.Z., Zulkifli, N.W.M., Masjuki, H.H., Kalam, M.A., Alabdulkarem, A.,
840 Gulzar, M., Khuong, L.S., Harith, M.H., 2017. A review on bio-based lubricants
841 and their applications. J. Clean. Prod. 168, 997–1016.
842 https://doi.org/10.1016/j.jclepro.2017.09.106
843 Tenorio-Alfonso, A., Sánchez, M.C., Franco, J.M., 2021. Impact of moisture curing
844 conditions on the chemical structure and rheological and ultimate adhesion
845 properties of polyurethane adhesives based on castor oil and cellulose acetate.
846 Prog. Org. Coatings 161, 106547. https://doi.org/10.1016/j.porgcoat.2021.106547
847 Tenorio-Alfonso, A., Sánchez, M.C., Franco, J.M., 2020. A Review of the Sustainable
848 Approaches in the Production of Bio-based Polyurethanes and Their Applications
849 in the Adhesive Field. J. Polym. Environ. 28, 749–774.
850 https://doi.org/10.1007/s10924-020-01659-1
851 Thyberg, K.L., Tonjes, D.J., 2016. Drivers of food waste and their implications for
852 sustainable policy development. Resour. Conserv. Recycl. 106, 110–123.
853 https://doi.org/10.1016/j.resconrec.2015.11.016
854 Tian, E., Mo, J., 2019. Toward energy saving and high efficiency through an optimized
855 use of a PET coarse filter: The development of a new electrostatically assisted air
856 filter. Energy Build. 186, 276–283. https://doi.org/10.1016/j.enbuild.2019.01.021
857 Webster, K., 2021. A Circular Economy Is About the Economy. Circ. Econ. Sustain. 1,
858 115–126. https://doi.org/10.1007/s43615-021-00034-z
859 Xu, A., Wang, Y., Xu, X., Xiao, Z., Liu, R., 2020. A Clean and Sustainable Cellulose-
860 Based Composite Film Reinforced with Waste Plastic Polyethylene Terephthalate.
861 Adv. Mater. Sci. Eng. 2020, 1–7. https://doi.org/10.1155/2020/7323521
862 Xu, H., Yagi, S., Ashour, S., Du, L., Hoque, M.E., Tan, L., 2023. A Review on Current
863 Nanofiber Technologies: Electrospinning, Centrifugal Spinning, and Electro-

Centrifugal Spinning. Macromol. Mater. Eng. 308. https://doi.org/10.1002/mame.202200502

Xue, J., Wu, T., Dai, Y., Xia, Y., 2019. Electrospinning and Electrospun Nanofibers: Methods, Materials, and Applications. Chem. Rev. 119, 5298–5415. https://doi.org/10.1021/acs.chemrev.8b00593

Yu, I.K.M., Chan, O.Y., Zhang, Q., Wang, L., Wong, K.-H., Tsang, D.C.W., 2023. Upcycling of Spent Tea Leaves and Spent Coffee Grounds into Sustainable 3D-Printing Materials: Natural Plasticization and Low-Energy Fabrication. ACS Sustain. Chem. Eng. 11, 6230–6240. https://doi.org/10.1021/acssuschemeng.2c07330

Zhang, J., Li, J., Wang, A., Edwards, B.J., Yin, H., Li, Z., Ding, Y., 2018. Improvement of the Tribological Properties of a Lithium-Based Grease by Addition of Graphene. J. Nanosci. Nanotechnol. 18, 7163–7169. https://doi.org/10.1166/jnn.2018.15511